Nocturnal low-level jets over shallow slopes

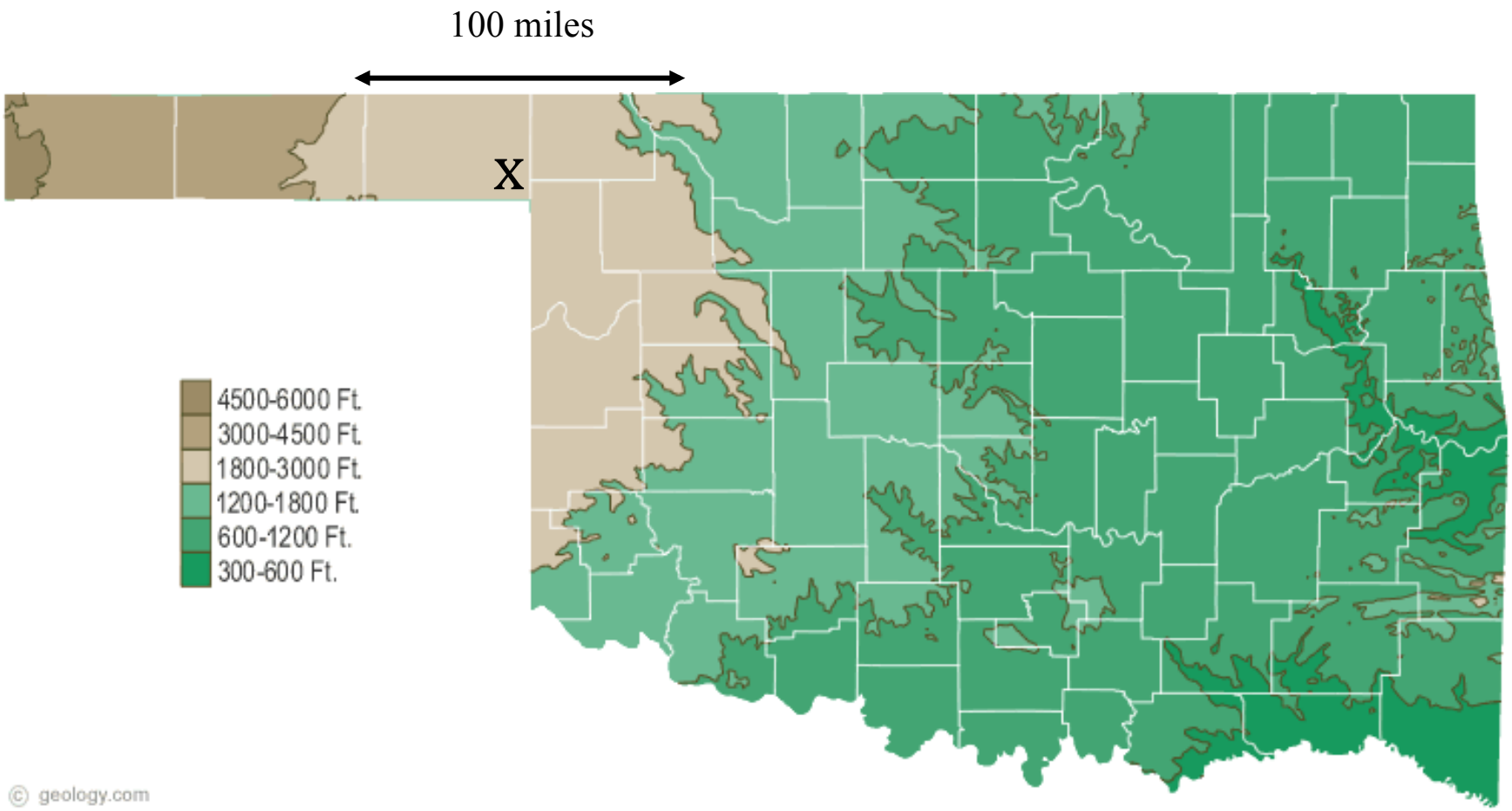

Slope of terrain near Slapout, OK ≈ (3000 ft - 1800 ft)/100 miles ≈ 0.0023 (≈ 0.15°)

Blackadar (1957) inertial oscillation theory for LLJs

Daytime
Boundary layer characterized by dry-convective mixing. Get a 3-way balance between pressure gradient force (PGF), Coriolis force, and friction (turbulent stresses).

Sunset
Rapid stabilization of boundary layer. Dry-convective mixing ceases. Turbulent stresses shut down. Flow is now unbalanced: parcels accelerate (initially in direction opposite the daytime friction force).

Nighttime
Coriolis force deflects the unbalanced flow. Get an inertial oscillation (IO), an anticyclonically turning circular hodograph.

Schematic of an inertial oscillation (after Blackadar 1957)

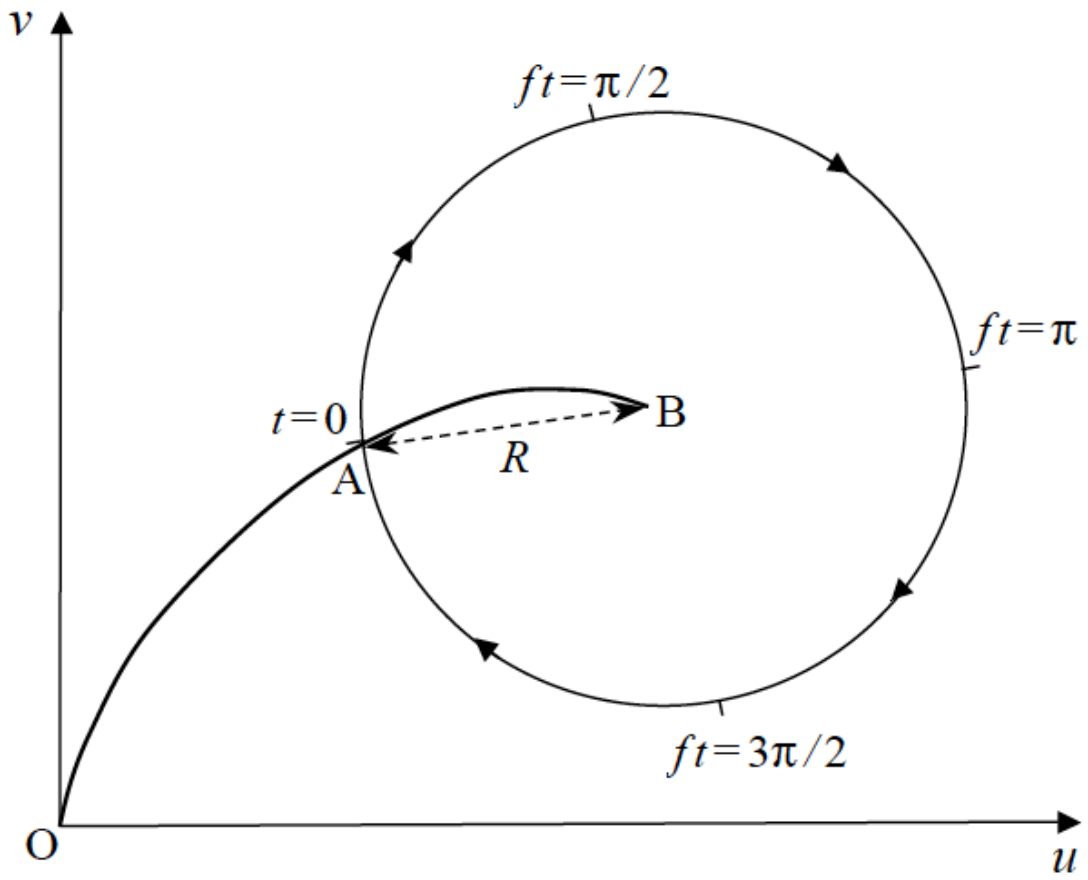

Curve OAB is daytime wind hodograph. Point B is the geostrophic wind at top of the boundary layer. The oscillation amplitude (radius R) is equal to the initial (sunset) ageostrophic wind speed.

Maximum LLJ wind speed in the Blackadar scenario

$$\vec{\text{wind}} = \vec{\text{geos}}_{\text{wind}} + \vec{\text{ageos}}_{\text{wind}}$$

At the ground (point O on Blackadar hodograph diagram) where the wind vector is 0 (no-slip), the ageostrophic wind is equal and opposite to the geostrophic wind (vector sum is 0).

Thus, the largest possible value of the ageostrophic wind speed (and therefore largest possible *R*) is the geostrophic wind speed.

Thus, the largest LLJ wind speeds possible in the Blackadar scenario are twice the geostrophic wind speed.

Limitations of the Blackadar theory

1. The theory cannot explain how peak winds in some LLJs exceed geostrophic values by > 100%

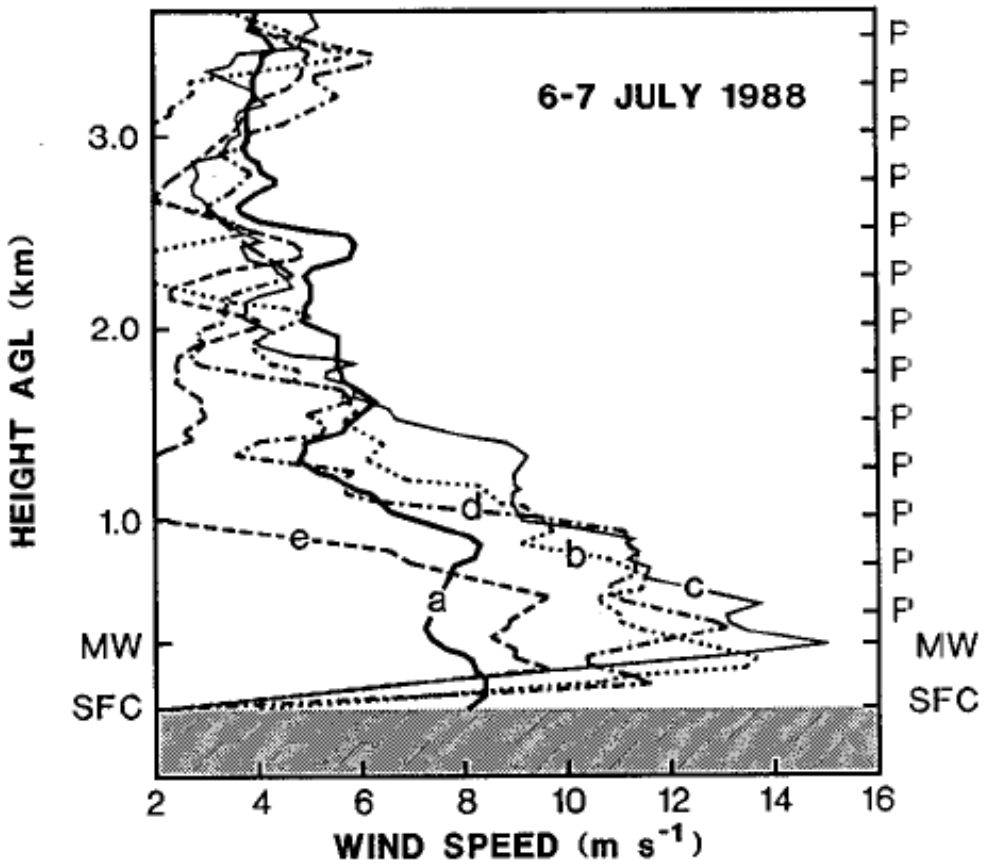

Wind speed vs height at Norman, OK from (a) 2331 UTC 6 July, (b) 0229 UTC 7 July, (c) 0535 UTC 7 July, (d) 0830 UTC 7 July, and (e) 1127 UTC 7 July (from Stensrud et al. 1990).

2. The theory cannot explain the geographical distribution of LLJs.

LLJ frequency (from Bonner 1968)

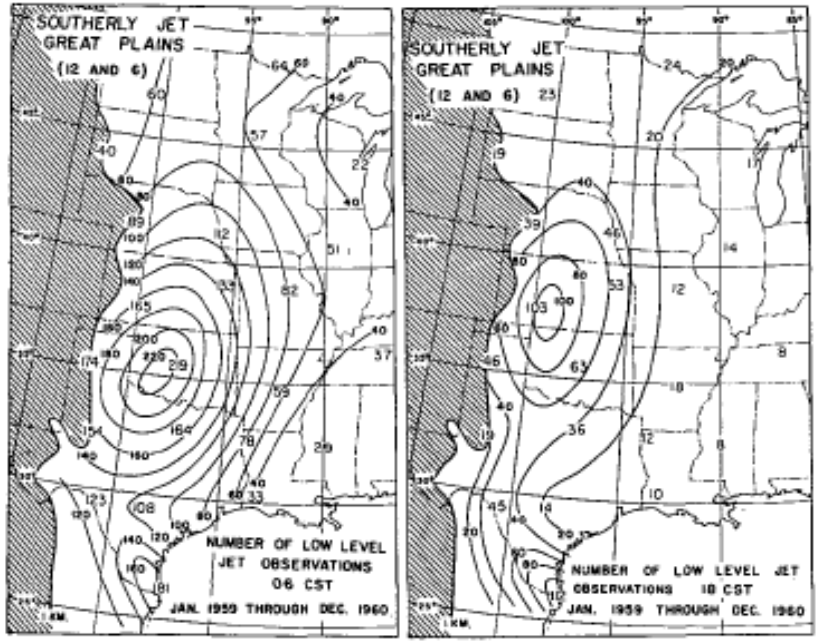

FIGURE 10.—Numbers of Criterion 1 "southerly jet" observations at 06 CST (left) and 18 CST (right). Two years of data.

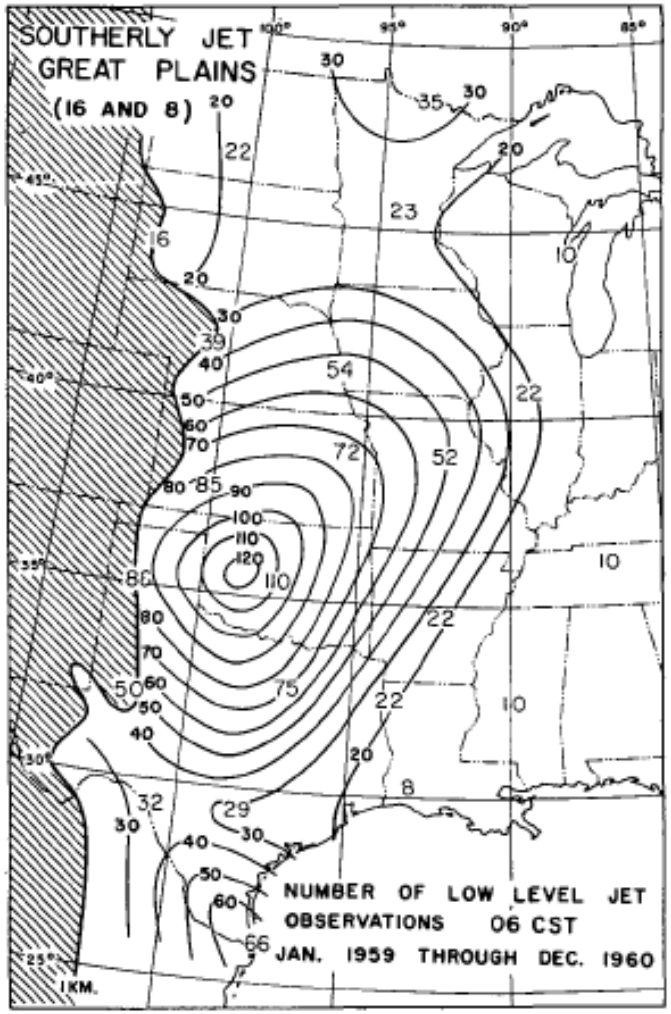

FIGURE 11.—Numbers of Criterion 2 "southerly jet" observations at 06 CST. Two years of data.

LLJ frequency (from Walters et al. 2008)

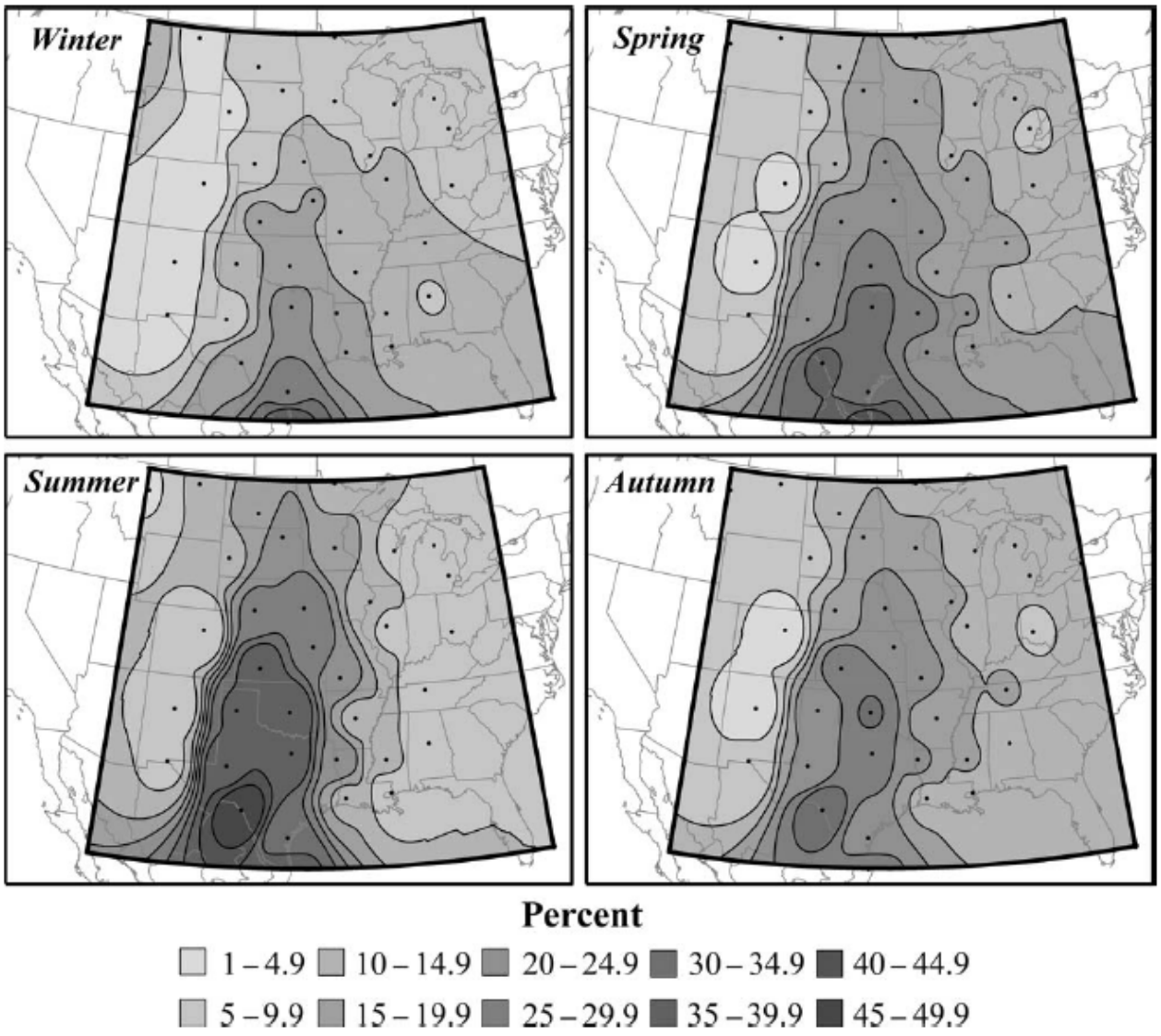

Figure 4. Frequency of southerly (113°–247°) low-level jets by season (expressed as percentage of the number of usable observations per season at each station). Jet frequencies were accumulated over both observation times (00 UTC and 12 UTC) and all intensity categories.

3. Daytime winds vary with z less than in Blackadar schematic

Daytime winds in Blackadar scenario:

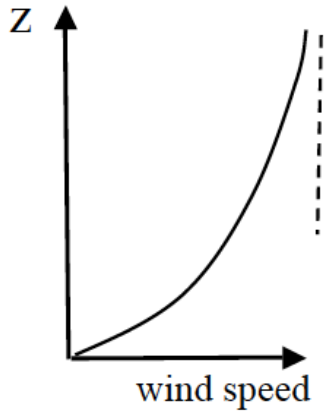

Peak LLJ winds in Blackadar scenario:

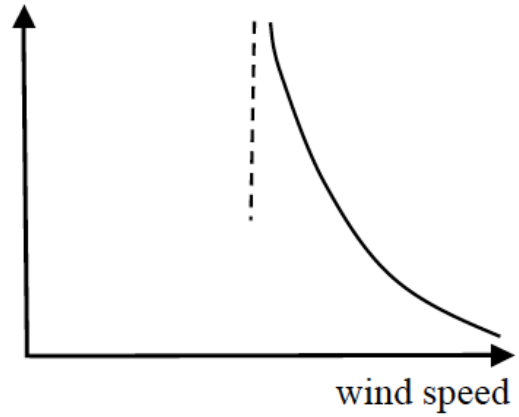

More realistic daytime winds:

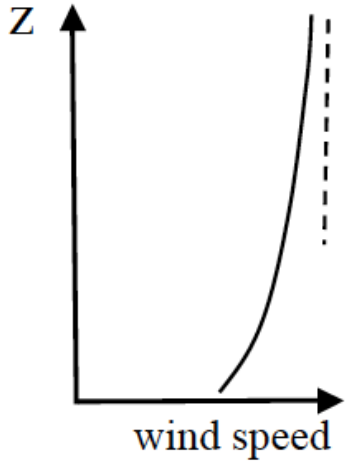

Peak LLJ winds when Blackadar-like theory is applied to those more realistic

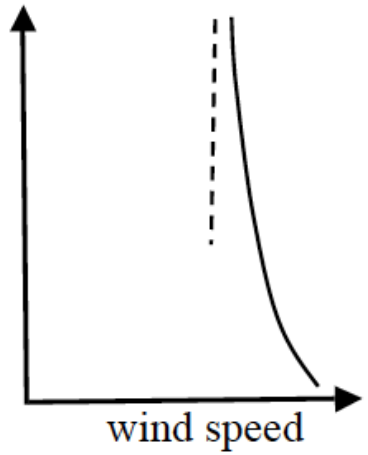

Given realistic daytime wind profiles, a Blackadar-like theory would yield broad, weak and not-very-jet-like LLJs.

Holton (1967) sloping boundary layer theory for LLJs

Viscous equations of motion and thermodynamic energy for a stably-stratified sloping boundary layer were solved analytically.

Attention restricted to spatially and temporally constant southerly geostrophic wind, and an imposed periodic (monochromatic, T = 24 hr) volumetric radiative forcing.

A diurnal wind oscillation was induced, but the results did not correctly reproduce the observed phase of the diurnal oscillations, and arguably the flow was not as jet-like as in observations.

Bonner and Paegle (1970) "sort-of" sloping boundary layer theory for LLJs

Considered time-varying eddy viscosity and geostrophic wind.

Periodicity of the geostrophic wind ascribed to diurnal temperature cycle over gently sloping terrain but analysis did not explicitly take terrain into account.

Results were in reasonable agreement with observations, but amplitude of the oscillation was very sensitive to the magnitude of the geostrophic wind, choice of viscosity, and phase difference between the viscosity and the geostrophic wind.

Shapiro and Fedorovich (2009; SF09) Tilted Residual Layer theory of Great Plains LLJs

Examined effects of terrain slope, thermal boundary layer structure, environmental stratification and synoptic-scale PGF on LLJ evolution.

Considered a very simple framework: extended the inviscid, 1D Blackadar theory to include slope angle and a coupling between the equations of motion and thermodynamic energy.

Treated LLJ as a response to the release of the frictional constraint near sunset, but considered the nature of the force(s) suddenly left unopposed to differ depending on a number of factors.

Now let's examine this SF09 theory in detail.

Problem formulation

Consider the development of a LLJ over a planar slope of infinite extent (no edges) having slope angle α. Work in slope-following Cartesian coordinates (as in our work with katabatic flow):

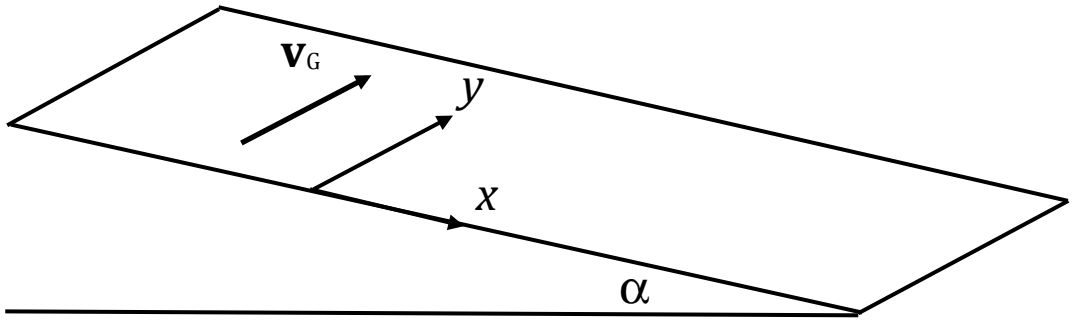

Restrict attention to (typical) case where synoptic-scale PGF points toward west, so geostrophic wind is southerly ($v_G > 0$), and treat f, v_G, N as constant. Same restrictions considered by Holton (1967).

Governing equations

$$\frac{du}{dt} = -b\sin\alpha + fv - fv_G, \tag{1}$$

$$\frac{dv}{dt} = -fu, \tag{2}$$

$$\frac{db}{dt} = uN^2\sin\alpha, \tag{3}$$

u, v are down- and cross-slope velocity components, respectively,

$b \equiv g(\theta - \theta_e)/\theta_r$, where θ_e is free-atmosphere potential temperature,

$N \equiv \sqrt{(g/\theta_r)d\theta_e/dz}$ is Brunt-Väisälä frequency,

v_G is geostrophic wind,

f is Coriolis parameter.

Terms in blue not accounted for in original Blackadar theory.

Free-atmosphere *N* versus local stratification

The *N* in (3) is environmental stratification. Local stratification will appear when we consider initial (sunset) conditions for parcel buoyancy.

Free-atmosphere *N* appearance in (3) means downslope derivative of q within boundary layer is being set to downslope derivative of q at top of boundary layer, i.e., in free atmosphere. This scenario underpins many 1D slope flow models (Prandtl 1942, Gutman & Malbakhov 1964, Rao & Snodgrass 1981, McNider 1982, Sorbjan 1989, Grisogono & Oerlemans 2001, Shapiro & Fedorovich 2008).
See also Fig. 12 of McNider and Pielke (1981).

Free-atmosphere *N* term in (3) yields warming in presence of downslope flow, and cooling in presence of upslope flow.

Potential temperature over a heated slope (from numerical simulation of McNider and Pielke 1981)

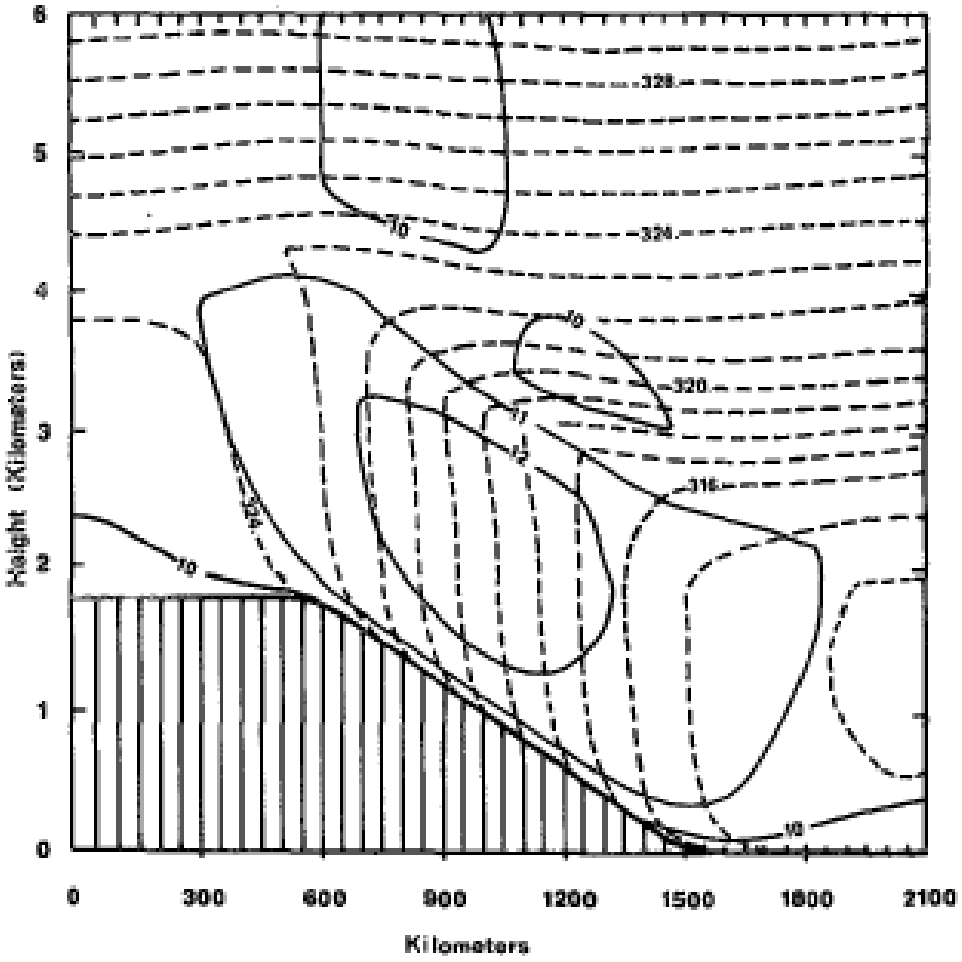

FIG. 12. Composite v component (solid) and potential temperature (dashed) contours at 1500 LST showing the development of the convective boundary layer and baroclinic zone over the sloping terrain for case 1. Contour intervals are 1 m s^{-1} and 1 K.

Solution for the hodograph

Use (2) to eliminate u in favor of v in (3), then integrate to get:

$$vN^2\sin\alpha + bf = const. \qquad (4)$$

Take u $\times$ (1) + $(v - v_G,) \times$ (2) + $b/N^2 \times$ (3), then integrate to get:

$$u^2 + (v - v_G)^2 + \frac{b^2}{N^2} = const. \qquad (5)$$

Eliminating b between (4) and (5) yields

$$u^2 + v^2(1 + N^2\sin^2\alpha/f^2) + mv = n, \qquad (6)$$

where m and n are functions of the parameters (not shown). Equation (6) describes an ellipse with major axis along the u-axis and minor axis along the v-axis. The ratio of major to minor axes is $\sqrt{1 + N^2\sin^2\alpha/f^2}$.

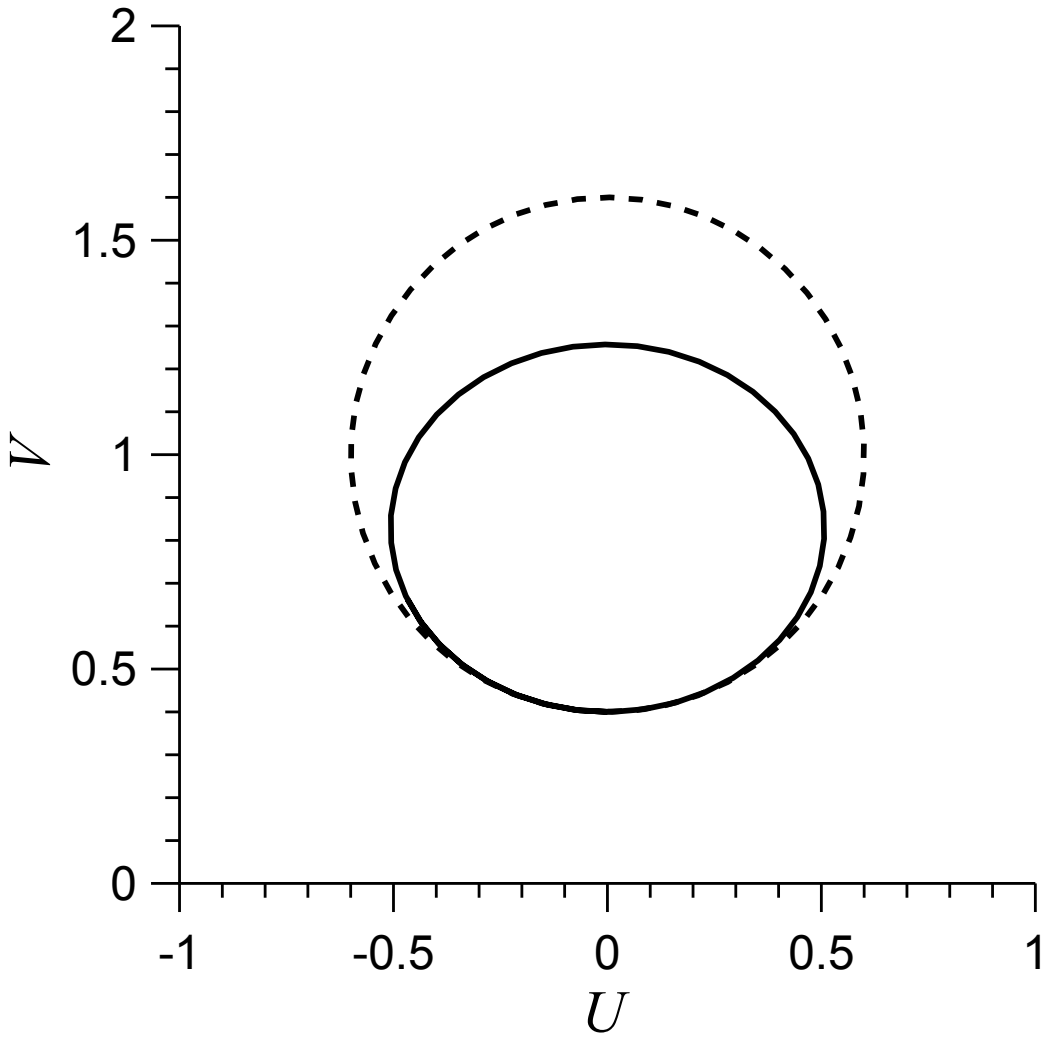

Hodographs of inertia-gravity oscillation over terrain at latitude 35°N with slope a = 0.2° for N=0 (dashed curve) and for $N = 0.015\text{s}^{-1}$ (solid curve). Downslope (U) and cross-slope (V) wind components are normalized by geostrophic wind speed. Hodographs correspond to same initial conditions: $B_0 = 0$, $U_0 = 0$, and $V_0 = 0.4$.

Predicted west/east elongation of LLJ hodographs is consistent with many observations of LLJs over the Great Plains.

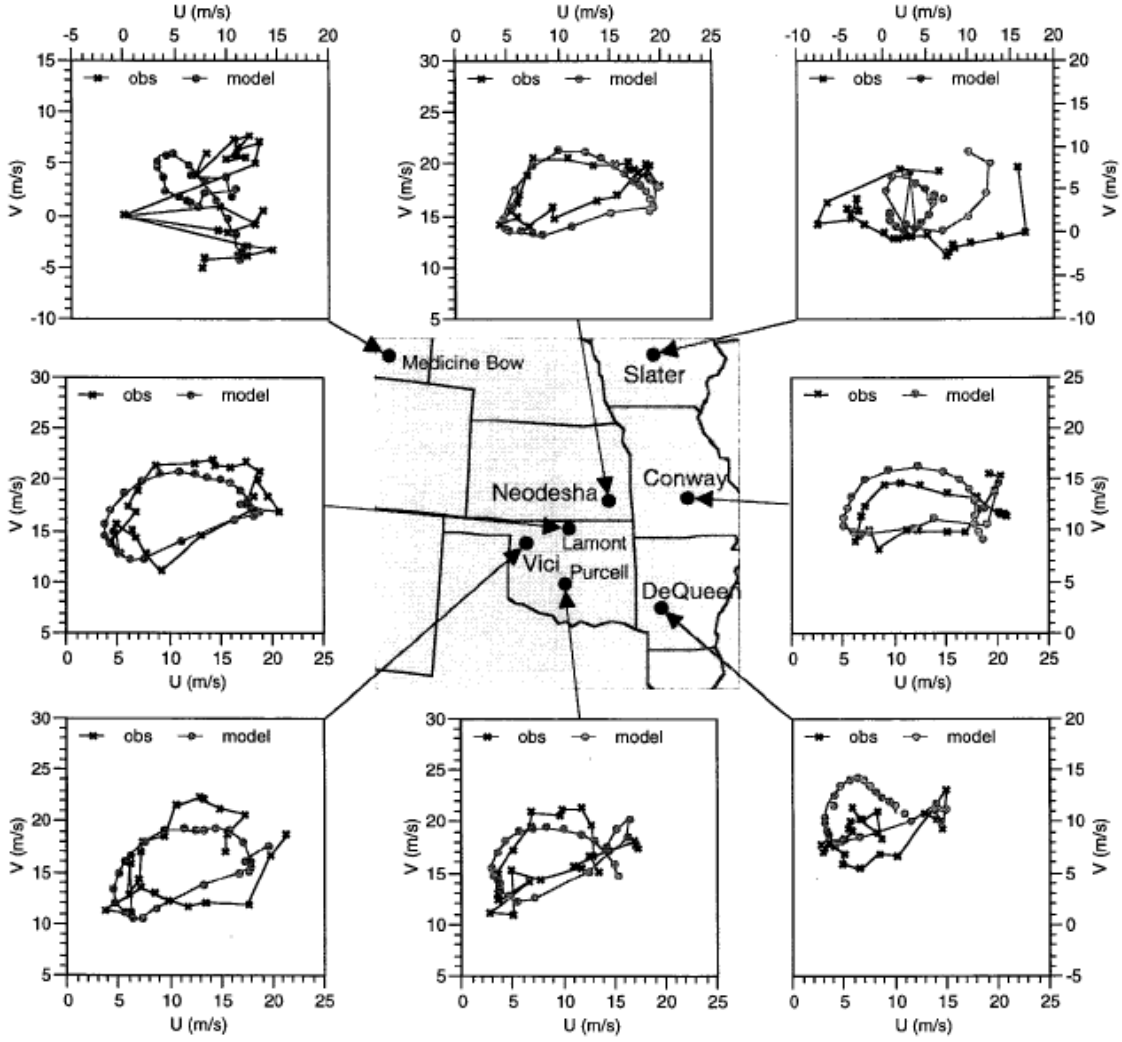

FIG. 7. Observed and simulated hodographs at the 867-m model level from 0700 CST 12 July to 0600 CST 13 July (1-h intervals) at several selected stations.

(from Zhong et al. 1996)

2 yr climatological hodograph from the Southern Great Plains Cloud and Radiation Testbed central facility in North-Central Oklahoma (from Whiteman et al. 1997)

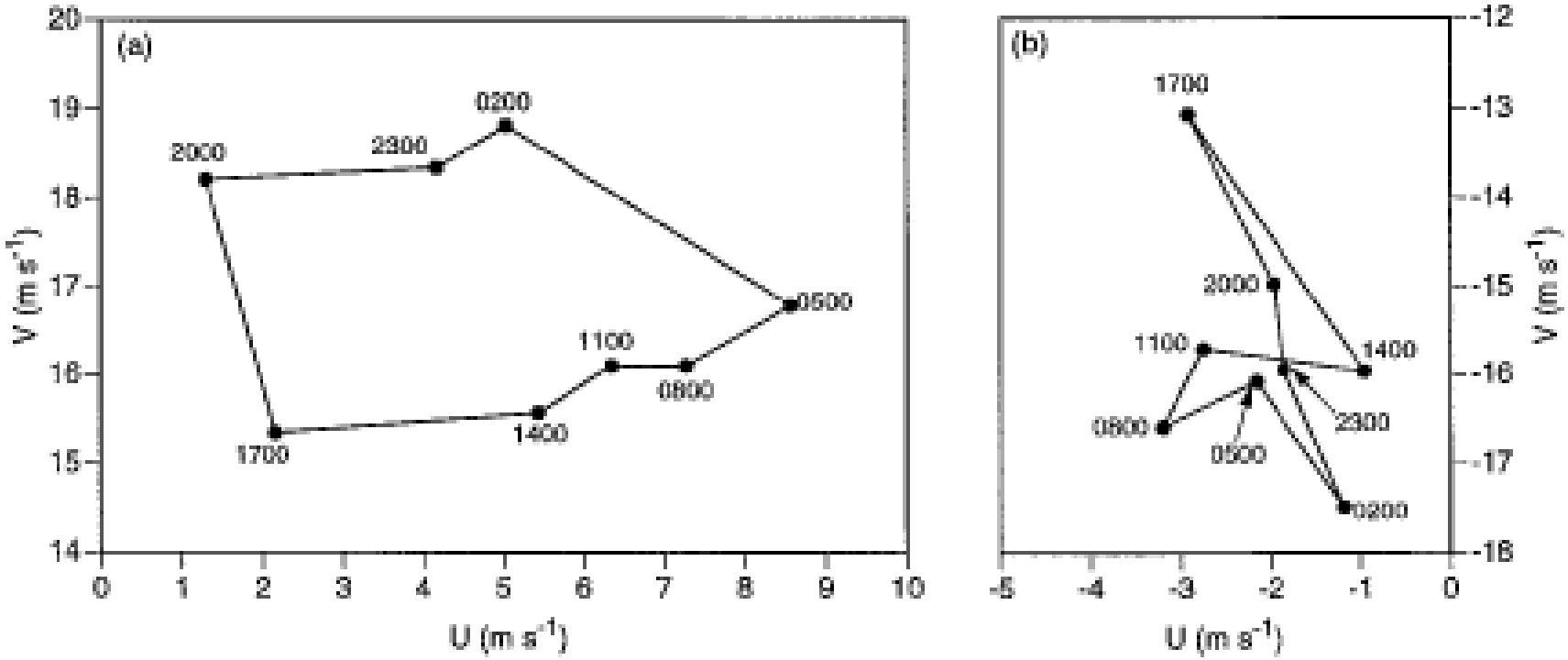

FIG. 14. Diurnal oscillations of wind speed and direction at the maximum jet wind level for (a) southerly and (b) northerly LLJs. The *U* represents the eastward wind speed component and *V* the northward component. Indicated times are central standard time.

6 yr climatological hodograph from Beaumont, KS (from Song et al. 2005)

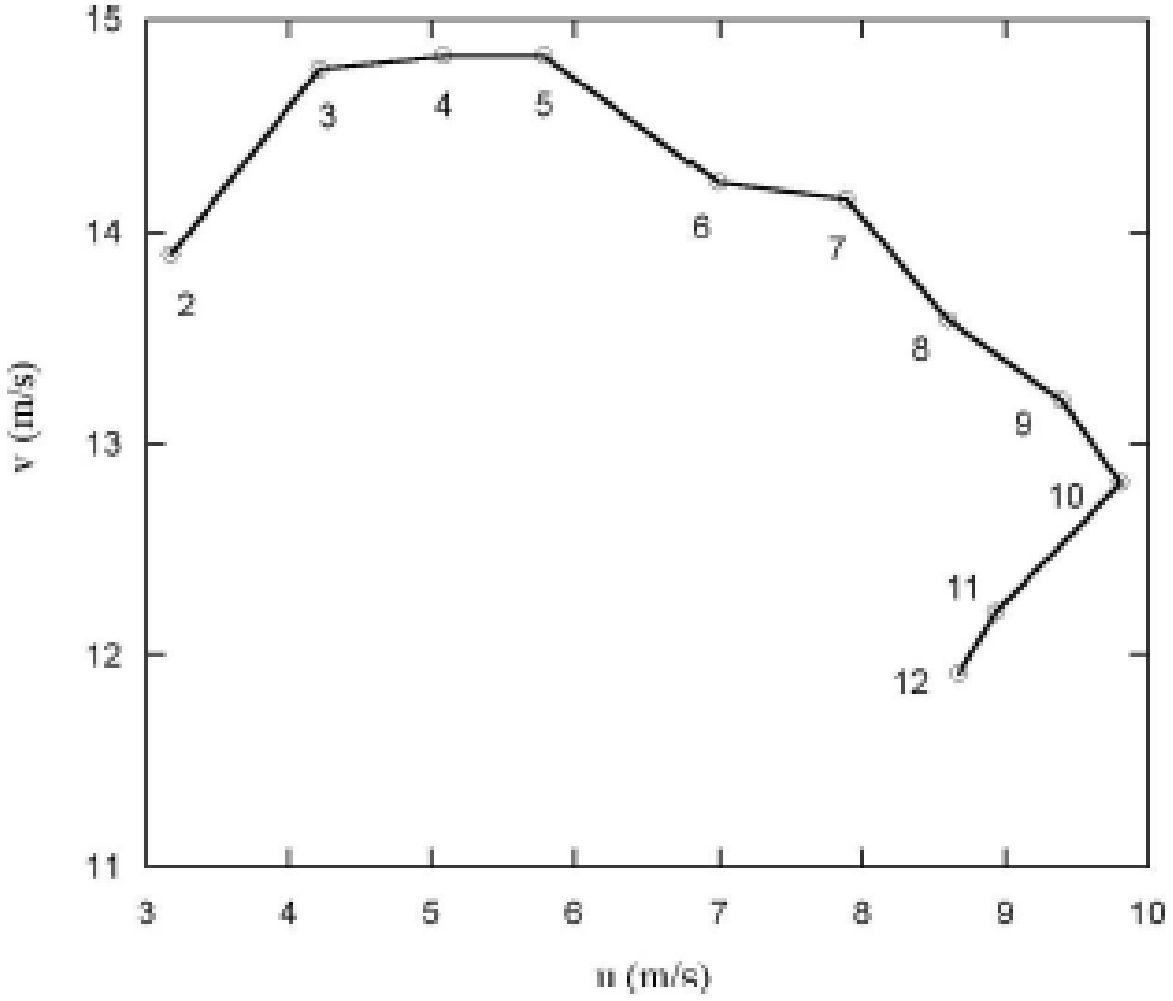

FIG. 8. Nocturnal variations (0200–1200 UTC) in the southerly LLJ hodograph for wind components averaged at the Beaumont site in the 6-yr hourly dataset.

Non-dimensionalization

Define:

$$\mathrm{Bu} \equiv \frac{N^2 \sin^2 \alpha}{f^2}, \text{ the slope Burger number,}$$

$$\Omega \equiv \sqrt{1 + \mathrm{Bu}}\,.$$

It is convenient to introduce the non-dimensional variables,

$$U \equiv \frac{u}{v_{\mathrm{G}}}, \quad V \equiv \frac{v}{v_{\mathrm{G}}}, \quad B \equiv \frac{b \sin\alpha}{f v_{\mathrm{G}}}, \quad T \equiv f t,$$

$$U_0 \equiv \frac{u_0}{v_{\mathrm{G}}}, \quad V_0 \equiv \frac{v_0}{v_{\mathrm{G}}}, \quad B_0 \equiv \frac{b_0 \sin\alpha}{f v_{\mathrm{G}}}.$$

Analytical solution of (1)-(3)

The solution for U, V, and B, expressed as deviations from their initial values is:

$$U(T)-U_0 = U_0\left(\cos\Omega T-1\right) + \frac{1}{\Omega}\left(-B_0+V_0-1\right)\sin\Omega T, \qquad (7)$$

$$V(T)-V_0 = -\frac{U_0}{\Omega}\sin\Omega T + \frac{1}{\Omega^2}\left(-B_0+V_0-1\right)\left(\cos\Omega T-1\right), \qquad (8)$$

$$B(T)-B_0 = \frac{\Omega^2-1}{\Omega}U_0\sin\Omega T - \frac{\Omega^2-1}{\Omega^2}\left(-B_0+V_0-1\right)\left(\cos\Omega T-1\right). \qquad (9)$$

B_0 and V_0 on the right hand sides of the solutions (7)-(9) always appear in the combination $-B_0+V_0$, so smaller initial southerly wind component (larger ageostrophic wind) is equivalent to larger positive initial buoyancy.

Reference values for slope angle

$\alpha = 0°$ Flat terrain. Problem reduces to Blackadar scenario.

$\alpha = 0.15°$ Characteristic slope of Texas/Oklahoma panhandles. Close to the 1/400 slope considered by Holton (1967).

$\alpha = 0.5°$ Upper bound for the terrain slope of the far western Great Plains.

$\alpha = 1°$ West of the Great Plains (i.e., in foothills somewhere)

Time series of U, V, B at latitude 35°N with N=0.01s^{-1} **with initial parcel buoyancy set to zero.**

Results shown for V_0=0.4 (solid lines) and V_0=0.8 (dashed lines).

Initial values U_0 and B_0 were set to 0.

slope angle: 0°

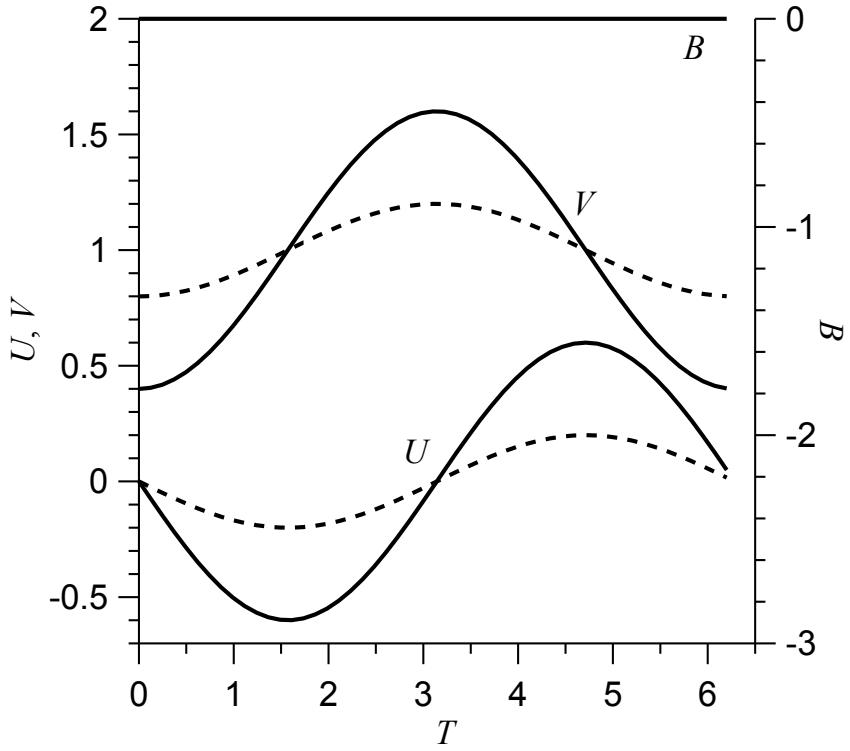

slope angle: 0.15°

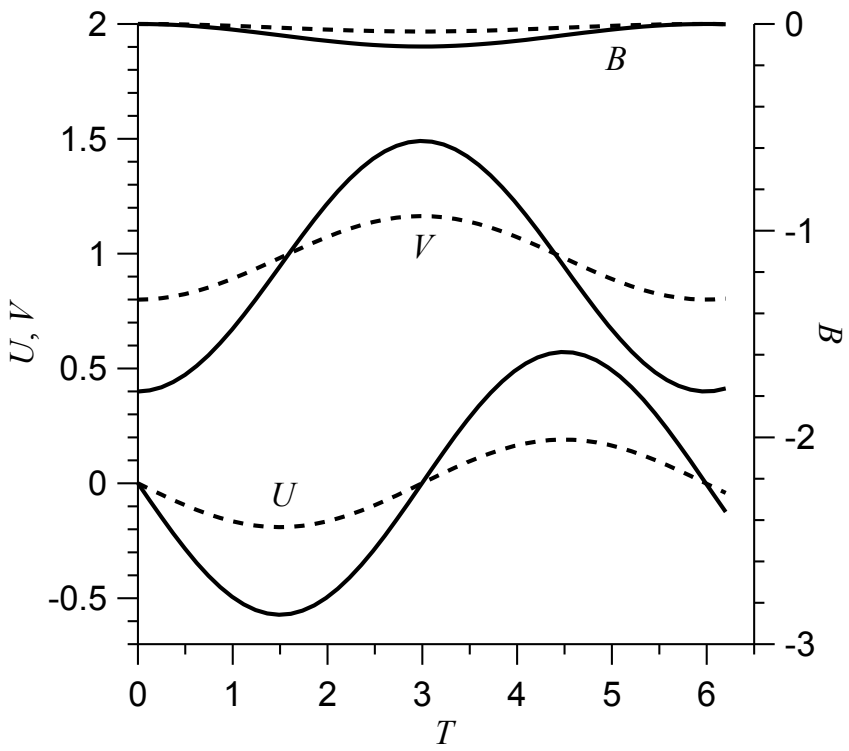

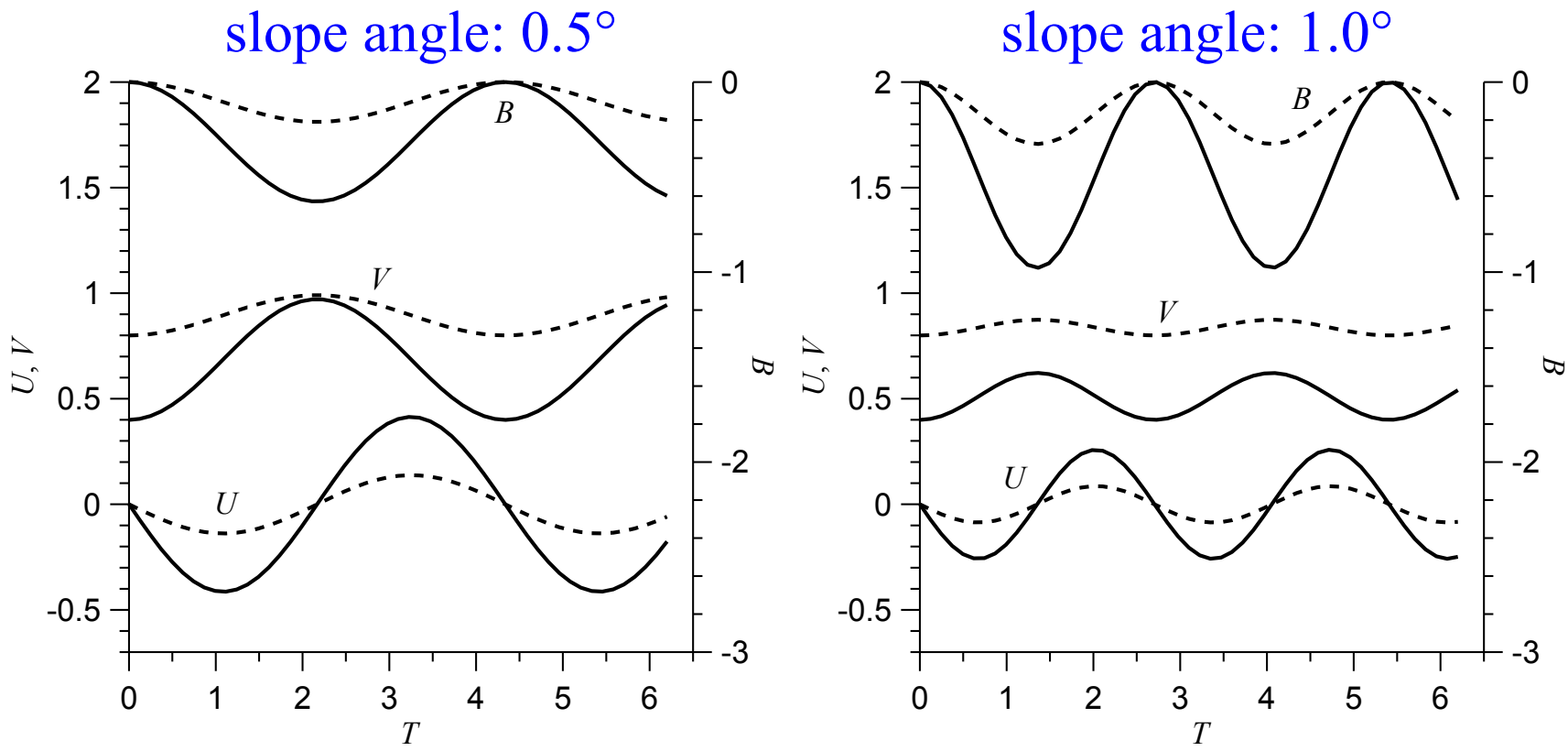

None of these results reveal a strong jet!

Results indicate peak jet winds weaken with slope angle.

What are appropriate B_0 for the Great Plains LLJ?

The dependence of low level jet strength on thermal structure of the boundary layer is implicit in our solution (initial value B_0), but how to specify B_0?

Idea:

(1) Adopt the notion of a residual layer (Stull 1988).

(2) But tilt it -- so we have a "tilted residual layer" (TRL).

(3) See what can be inferred about B_0 from the TRL. Recall definition of parcel buoyancy: it's proportional to difference in θ between parcel and environment at the same elevation.

Diurnal cycle of the planetary boundary layer

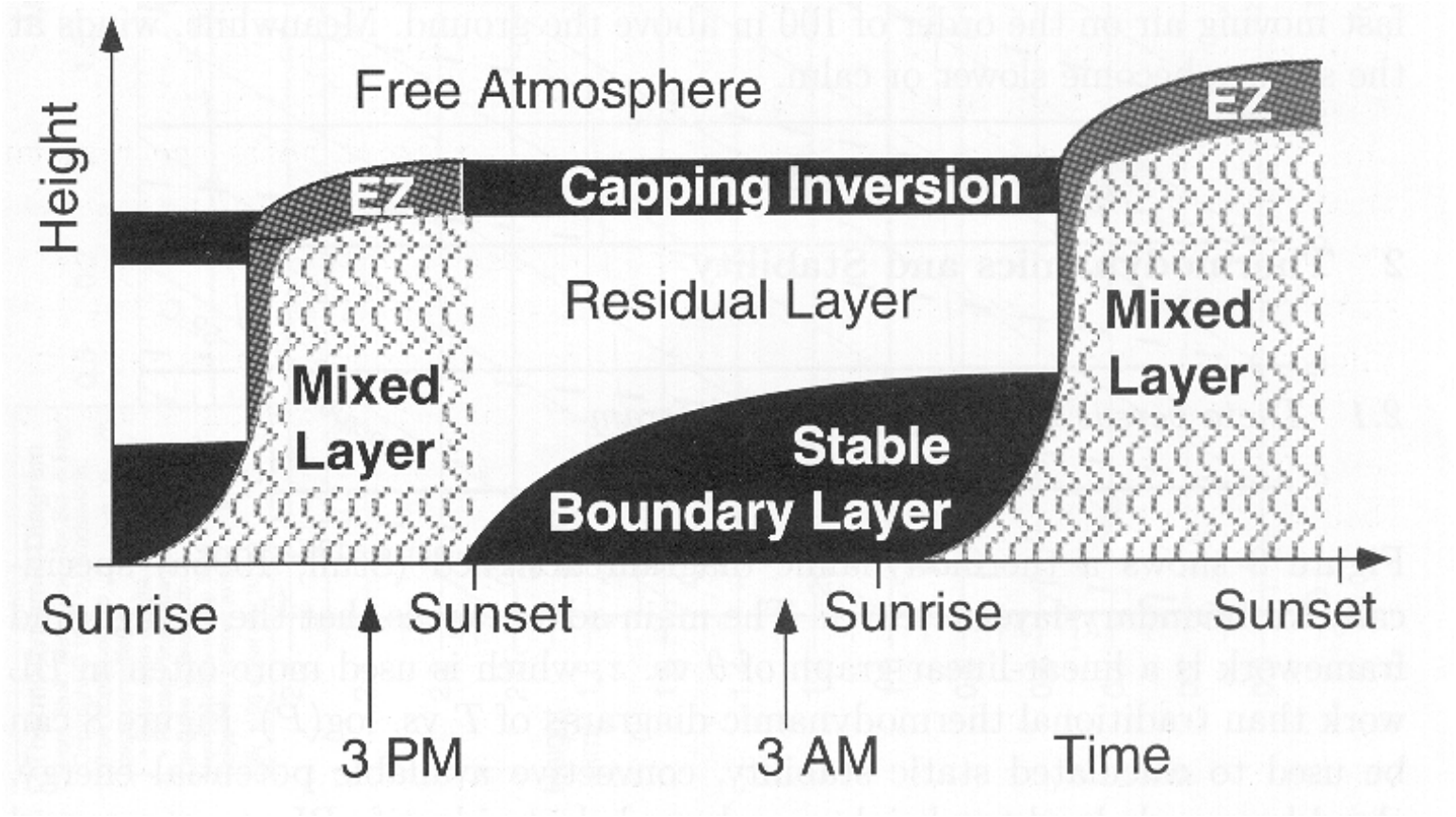

(from Stull 1998, article in "Clear and Cloudy Boundary Layers")

Anatomy of a tilted residual layer (TRL)

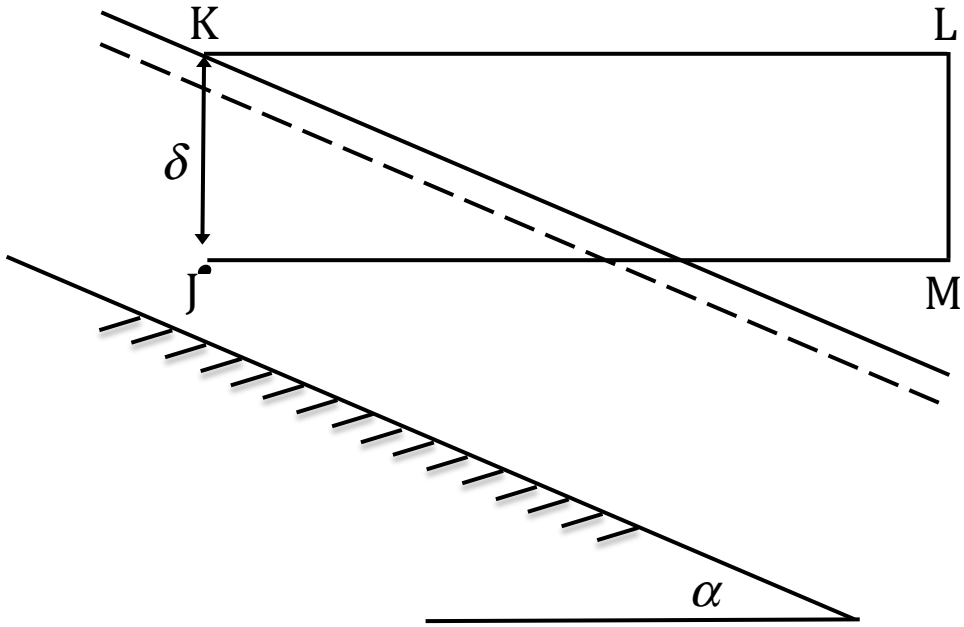

Vertical slice through TRL. Dashed line is base of inversion. Sloping solid line through K is top of inversion. J is an air parcel. δ is distance of parcel from top of inversion. L is in free atmosphere at same elevation as K. M is in free atmosphere at same elevation as J. Horizontal line KL is an environmental isentrope.

Estimating B_0 in a TRL

θ is approximately constant ($=\theta_0$) from J up to base of inversion, and then increases by $\Delta\theta$ across interface. So θ at K is $\theta_0 + \Delta\theta$.

Since KL is an environmental isentrope, θ at L is also $\theta_0 + \Delta\theta$.

$\theta \downarrow$ from L to M by an amount equal to the environmental potential temperature gradient $d\theta_e/dz$ times the altitude difference δ (> 0) between L and M. So θ at M is $\theta_0 + \Delta\theta - \delta\, d\theta_e/dz$.

Thus, the initial buoyancy for the parcel at J is $b_0 = -g\Delta\theta/\theta_r + N^2\delta$, and the corresponding non-dimensional buoyancy is:

$$B_0 = \frac{N^2 \sin\alpha}{f v_G}\delta - \frac{\sin\alpha}{f v_G}\frac{g\Delta\theta}{\theta_r}. \qquad (10)$$

Implications of the B_0 formula

For values of the parameters typical of the Great Plains boundary layer, B_0 is very sensitive to all of the parameters in (10).

At locations slightly beneath the capping inversion, δ is small and (10) indicates parcels there have negative buoyancy.

For parcels at low levels (e.g., where LLJ occur), (10) indicates the buoyancy is positive. Also: larger N associated with larger B_0!

So, TRL has a downward-directed buoyancy gradient, and therefore a means for a "jet-like" profile to evolve from a well-mixed (with respect to momentum and θ) initial state.

Peak LLJ wind speeds in the TRL model

Applying (10) in (8) at the time $T = \pi/\Omega$ when V attains a peak amplitude $V_{\max}$ (taking $U_0 = 0$) yields

$$V_{\max} = \frac{2f^2}{f^2+N^2\sin^2\alpha}\left(\frac{N^2\sin\alpha}{f v_G}\delta - \frac{\sin\alpha}{f v_G}\frac{g\Delta\theta}{\theta_r} + 1\right) + V_0\left(1 - \frac{2f^2}{f^2+N^2\sin^2\alpha}\right) \qquad (11)$$

Eq. (11) yields large $V_{\max}$ for parcels with small V_0 (large initial ageostrophic wind speed $1-V_0$) located at low levels (large δ) within a TRL with a weak capping inversion (small $\Delta\theta$).

V_{max} as a function of slope angle α for a parcel with $V_0 = 0.4$

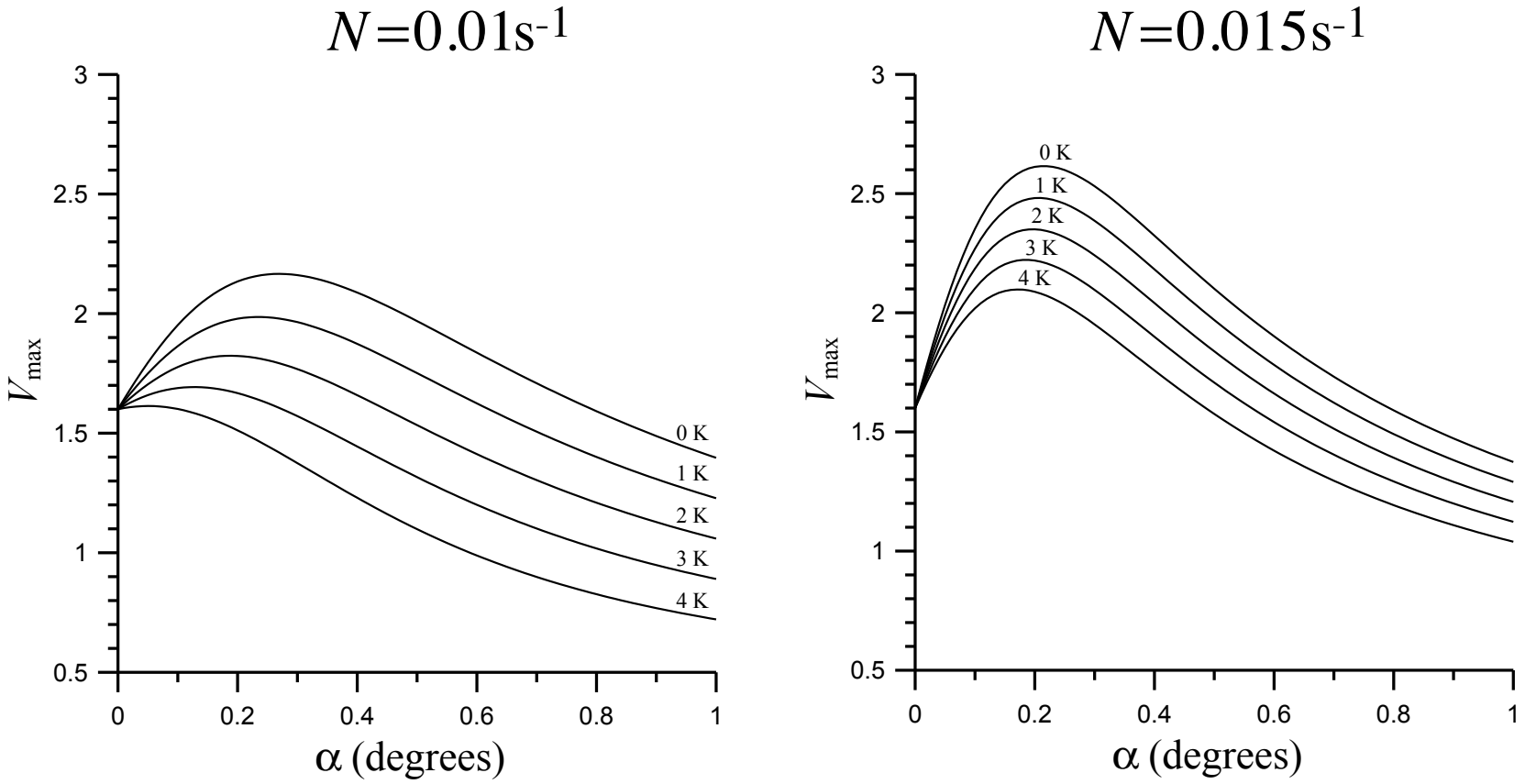

Parcel located 1000 m beneath a capping inversion. Results shown for five capping inversion strengths, $\Delta\theta = 0, 1, 2, 3, 4$ K.

V_{max} as a function of slope angle α for a parcel with $V_0 = 0.8$

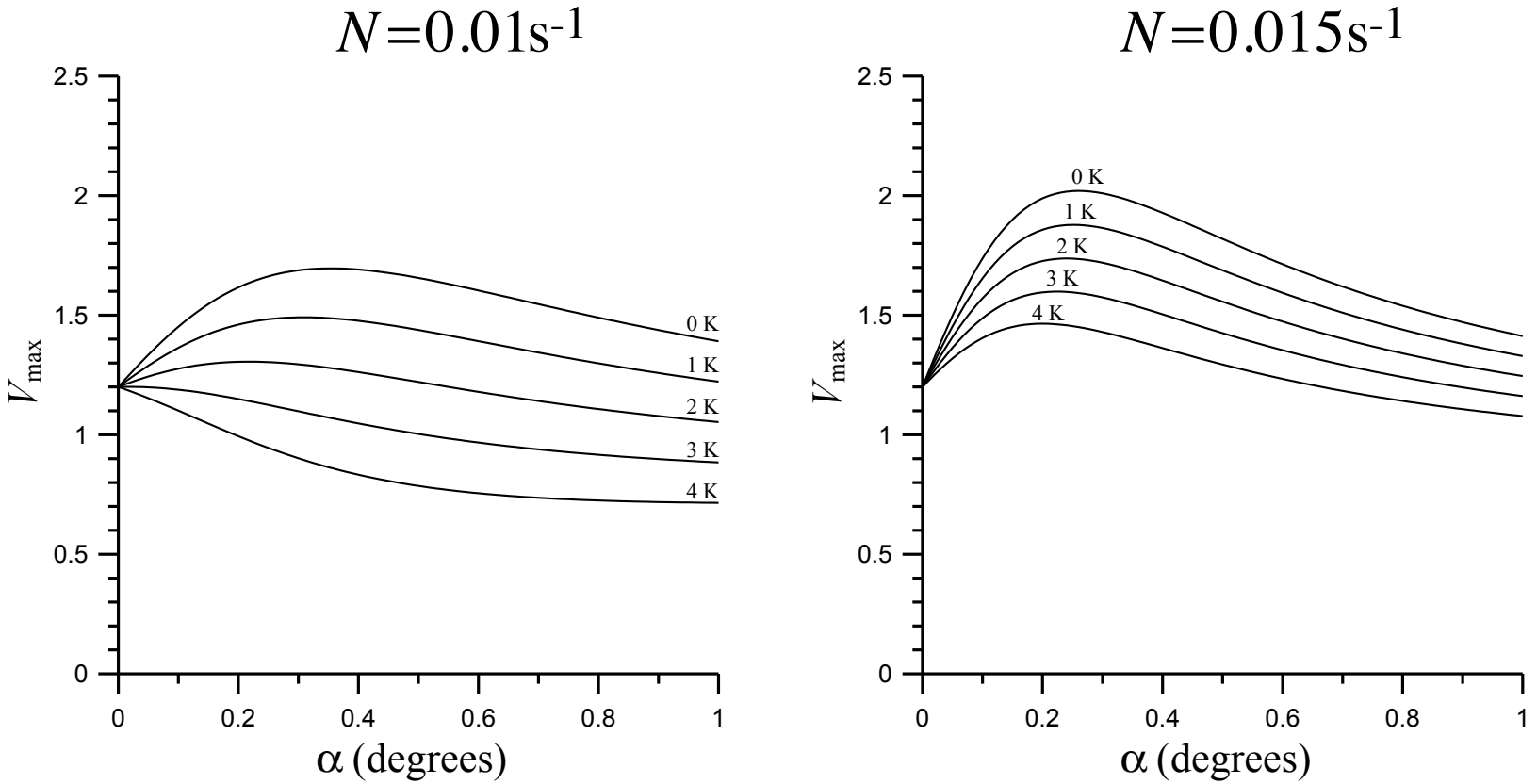

Parcel located 1000 m beneath a capping inversion. Results shown for five capping inversion strengths, $\Delta\theta = 0$, 1, 2, 3, 4 K.

Optimum slope angle

The slope angle α^* at which $V_{\max}$ is largest is obtained from $(dV_{\max}/d\alpha)\big|_{\alpha=\alpha^*} = 0$ as

$$\alpha^* = -\frac{f v_G (1-V_0)}{N^2\delta - g\Delta\theta/\theta_r} + \sqrt{\left(\frac{f v_G (1-V_0)}{N^2\delta - g\Delta\theta/\theta_r}\right)^2 + \frac{f^2}{N^2}}. \qquad (12)$$

α^* is roughly in the 0.10°–0.20° range for $V_0 = 0.4$,

α^* is roughly in the 0.15°–0.25° range for $V_0 = 0.8$.

Qualitatively good agreement with climatological studies ... but the more reasonable case ($V_0 = 0.8$) yields an optimum slope angle associated with terrain west of the panhandles (i.e., too far west).

Summary of main results

- Jet evolves on hodograph as an ellipse with major axis aligned with *u*-wind component. Result is consistent with observations.

- Very strongly supergeostrophic winds observed in some real jets can only be accounted for in our theory by including terrain and initial buoyancy (following proposed TRL model).

- Initial (sunset) buoyancy profile within the TRL provides conditions for flow to develop a jet-like velocity profile from a well-mixed (uniform) initial velocity field.

- The theory predicts the existence of an optimum slope angle associated with peak jet strength. This result is qualitatively consistent with climatological studies.